Effect of RF Pulse Sequence on Temperature Elevation for a Given Time-Average SAR

ZHANGWEI WANG,[1] CHRISTOPHER M. COLLINS[2]

[1] *GE Healthcare, Aurora, OH 44202*
[2] *Department of Radiology and Bioengineering, The Pennsylvania State University, Hershey, PA 17033*

ABSTRACT: In calculations of temperature increase during MRI, it is typically assumed adequate to consider the specific energy absorption rate (SAR) levels averaged over an entire repetition time (TR) rather than explicitly consider the heating (as it occurs in reality) during the RF pulses only. Here, we investigate this assumption with numerical calculations of SAR and temperature increase for a human head in a volume coil at 64 and 300 MHz during three very different pulse sequences, each having a TR of 200 ms and a time-average whole-head SAR of 3.0 W/kg, as well as with semianalytical calculations considering a gradient-echo sequence in a segment of tissue with SAR of 10 W/kg delivered in a 1-ms pulse with TR of up to 5,000 ms. Although it is possible to calculate a temporal effect of specific pulse sequence on temperature, the difference between pulse sequences is so small and so transient that it should typically be adequate to consider only the time-average SAR in each TR. Concepts Magn Reson Part B (Magn Reson Engineering) 37B: 215–219, 2010

KEY WORDS: MRI; pulse sequence; SAR; temperature

INTRODUCTION

In an MRI exam, the patient is exposed to numerous pulses of RF energy, which introduce heat into the tissue. To minimize the risk of inducing hyperthermic tissue damage, regulatory bodies have established limits on the specific energy absorption rate (SAR) averaged over any 10-g region of tissue, the whole-body, whole-head, and/or partial body as appropriate for the region exposed to the RF fields (*1*). Although SAR can serve as the driving source of tissue temperature elevation, it is not SAR itself, but the temperature experienced by the tissue over time can cause damage. SAR and temperature can have a fairly complex relationship (*2–6*), and regulatory bodies have also recommended limits for local and core body temperature increases (*1*).

Recently, some investigators have calculated temperature increase in the human body due to RF heating in MRI using numerical methods (*2–6*). It has been shown that concentrating all the RF energy into the first 2 min of consecutive 6-min intervals can result in significantly higher transient temperature elevations than when the energy is applied evenly over time (*5*). Although it is commonly assumed that the pulsatile nature of the RF energy during each repetition time (TR) during an MR pulse sequence should not similarly affect the temperature distribution, a dedicated study of this has not previously been published.

METHOD

Full-Maxwell calculations of the electromagnetic fields produced throughout the head were performed using a home-built implementation (*7*) of the finite

Received 3 February 2010; revised 13 May 2010; accepted 26 July 2010

Correspondence to: Christopher M. Collins; E-mail: cmcollins@psu.edu

Concepts in Magnetic Resonance Part B (Magnetic Resonance Engineering), Vol. 37B(4) 215–219 (2010)

Published online in Wiley Online Library (wileyonlinelibrary.com). DOI 10.1002/cmr.b.20172

Figure 1 Coil and head model geometry on the axial, sagittal, and coronal planes passing through the coil center. Figures with greater detail have been published previously (*6*).

difference time domain (FDTD) method for electromagnetics (*8*). Details of the FDTD calculations have been provided elsewhere (*6*). In brief, the head model had a resolution of 3 mm in each dimension. The RF coil was modeled after a TEM resonator (*9*) with multiple sources to achieve a current distribution such that all rungs had equal current magnitude and current phase proportional to angle of location in the azimuthal plane. The coil had an inner diameter (distance between rungs on opposite sides of coil) of 28 cm, an outer (shield) diameter of 33 cm, and a length of 19 cm. The geometry of the head in the coil on central axial, sagittal, and coronal planes is shown in Fig. 1. Calculations were performed at 64 and 300 MHz corresponding to MRI at 1.5 and 7.0 T static magnetic field strengths. Electrical properties of tissue were derived from the literature using a four Cole–Cole fitting technique and parameters published previously (*10*). The SAR was calculated from the electric field as

$$\mathrm{SAR} = \sigma|E|^2/2\rho, \qquad [1]$$

where E is the peak electric field strength, σ is the local tissue conductivity, and ρ is the local tissue mass density.

Temperature was calculated with a finite difference implementation of the Pennes bioheat equation (*11*)

$$C_p\rho\frac{\partial T}{\partial t} = \nabla(K\nabla T) + \rho\mathrm{SAR} + A - B(T - T_b) \qquad [2]$$

and an established convection-based boundary condition (*12*). Here, t is time, T is local temperature at time t, C_p is the local specific heat, K is the local thermal conductivity, B is local tissue perfusion coefficient, T_b is the blood temperature, and A is the metabolic rate of heat production. In the finite difference implementation, 3-mm spatial resolution and 0.1-ms temporal resolution were used.

The different values for material density, heat capacity, thermal conductivity, perfusion by blood, and heat of metabolism for white matter, gray matter, blood, bone, muscle, fat, and skin were acquired from the literature (*2–6*, *12–14*). It was assumed that the rate of perfusion was independent of time and temperature (*15*), the T_b was constant at 37°C, and ambient temperature was 24°C. An initial equilibrium temperature distribution was first calculated with SAR = 0 W/kg. Then, the RF field was normalized as to induce 3.0 W/kg head-average SAR over time for each of three RF pulse sequences: 1) continuous wave (CW), 2) multispin echo (ME) having the RF energy concentrated into only six pulses (a 3-ms excitation pulse and five 1.5-ms refocusing pulses) during each 200-ms TR, and 3) gradient-refocused echo (GE) having the energy concentrated into a single 1.0-ms pulse during each 200-ms TR. The temperature increase through time was calculated during 10 min of heating with each of the three RF pulse sequences at both 64 and 300 MHz. The head-average SAR during the pulse sequences is shown in Fig. 2.

In addition to these purely numerical methods, semianalytical calculations were performed to explore a conservative scenario of a gradient-echo sequence with all the energy deposited during a 1-ms pulse and TR ranging from 1 to 5,000 ms with no thermal conduction allowed and with a time-average local SAR of 10 W/kg. In this case ($K = 0$), Eq. [2] is reduced to a linear first-order differential equation yielding

$$T = T_b + \frac{\rho\mathrm{SAR}}{B} + \frac{A}{B} + De^{-\frac{B}{\rho C_p}(t-t_s)}, \qquad [3]$$

where t_s is the time of the last change in SAR. An expression for D (found by considering the case when $t - t_s$ in Eq. [3] approaches infinity) is seen to be the difference between the tissue temperature at t_s

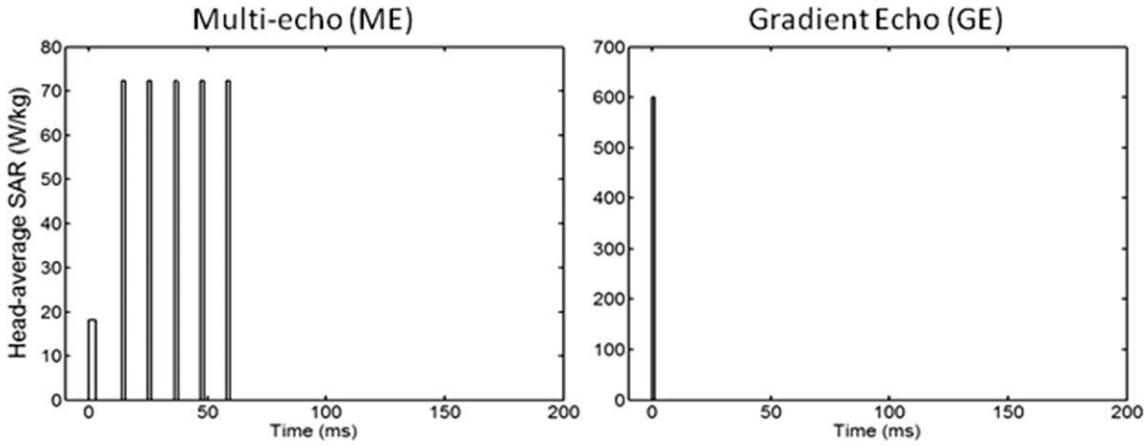

Figure 2 Head-average SAR for different sequences simulated. Left: Multiple spin echo (ME) with TR = 200 ms and TE = 11 ms; the duration of 90° and 180° pulse is 3 and 1.5 ms, respectively. Right: Gradient echo (GE) at TR = 200 ms and pulse duration of 1 ms. Also simulated (but not shown in this figure) was a continuous-wave (CW) excitation. For all sequences, the time-average SAR over the head is 3 W/kg.

(T_s) and the equilibrium value for T (when $t - t_s$ in Eq. [3] approaches infinity) with the current value of SAR:

$$D = T_s - \left(T_b + \frac{\rho SAR}{B} + \frac{A}{B}\right). \qquad [4]$$

Using Matlab (The Mathworks, Natick, MA), an algorithm was implemented to calculate T using these analytical equations as SAR was alternately set to 10 W/kg multiplied by TR/1 ms for a duration of 1 ms and then to 0 W/kg for a period of TR minus 1 ms. Starting with T at equilibrium for SAR = 0 ($T = T_b + A/B$), for each value of TR, the calculation was performed until t reached 2 h, and the maximum change in temperature during any single repetition for each value of TR was determined. This entire process was repeated for values of TR ranging from

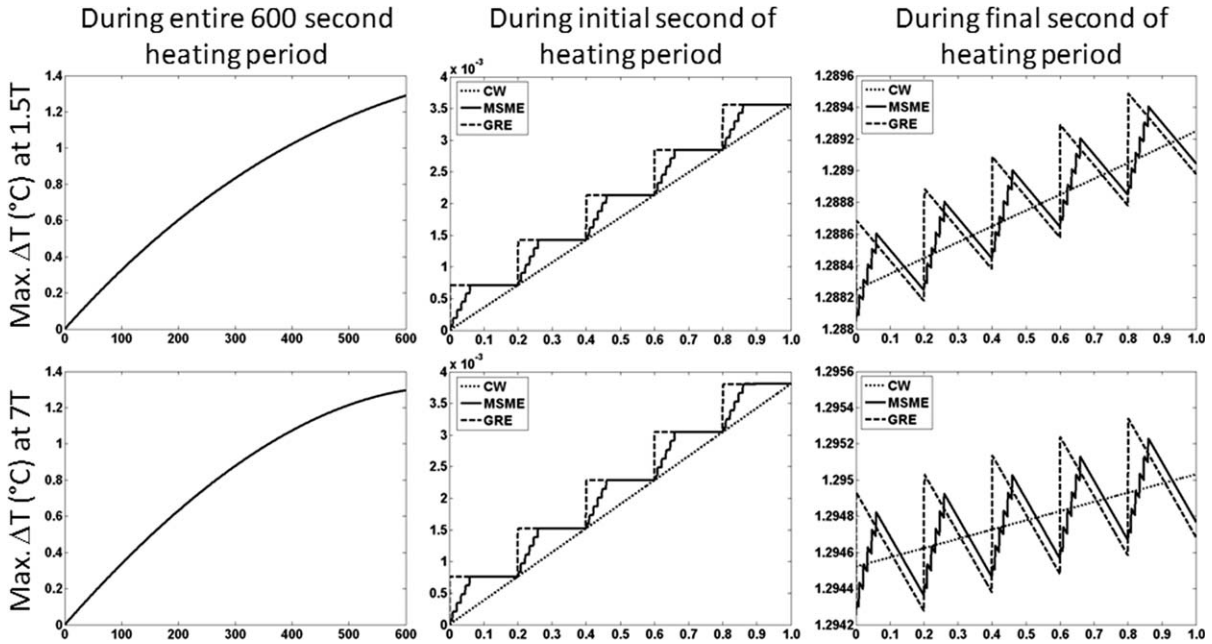

Figure 3 The temperature rise above baseline at the location of maximum temperature change during the entire time course (left), during the first 1 s (center), and during the last 1 s (right) of a 10-min exposure to 3.0 W/kg head-average SAR at 64 (top) and 300 MHz (bottom).

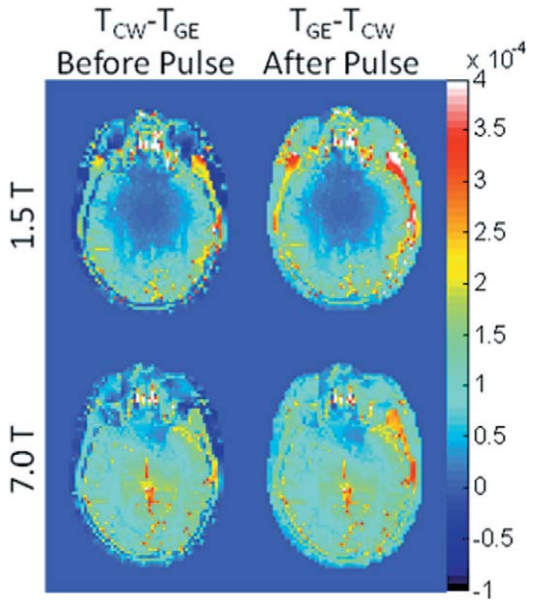

Figure 4 Temperature difference between CW and ME sequences on an axial plane passing through the eyes immediately before (left) and immediately after (right) a single RF pulse of the GE sequence applied near the end of the 10-min period of heating at both 64 (top) and 300 MHz (bottom). [Color figure can be viewed in the online issue, which is available at wileyonlinelibrary.com.]

1 (CW) to 5,000 ms. For this analysis, properties of muscle tissue were used (*6*): $\rho = 1{,}047$ kg/m^3, $C_p =$ 3,600 W/(kg °C), $A = 480$ W/m^3, and $B = 3{,}360$ W/(m^3 °C). A constant T_b of 37°C was assumed.

RESULTS AND DISCUSSION

For any of the three pulse sequences simulated here, overall trends in the temperature distribution with time during application of SAR at each frequency were similar to those reported previously in similar calculations with a CW sequence (*6*). In preliminary calculations, we found that after 10 min of heating, the level of temperature increase at the center of the head was ~90% of the value at thermal equilibrium. Because in this work, head-average SAR was the same at each frequency, no major increase in temperature when going from 3 to 7 T is expected. If, alternatively, a certain B_1 field strength was maintained, greater SAR values and temperature increases would certainly be expected at 7 T than at 3 T.

Figure 3 shows the elevation of temperature above the baseline level with time for all three pulse sequences at the location of greatest temperature increase for both 64 (1.5 T) and 300 MHz (7 T) excitations. When examining the entire 10-min time course simulated (plots on left side of Fig. 3), no difference between the pulse sequences can be seen. Close examination of the time courses (such as during the first and last seconds of heating shown in center and right side plots of Fig. 3), however, reveals slight difference in temperature depending on the sequence. The magnitude of these differences is less than 1×10^{-3}°C. Effects of thermal conduction and perfusion have a greater cooling effect at the end of the exposure period, when the temperature is above the initial levels, so that at times when no RF energy is applied, the temperature in the GRE and MSME sequences can dip below that in the CW sequence. The location of greatest temperature increase occurs in the right-hand masticator space at the level of the zygomatic arch at 1.5 T and in the neck near the right-hand trapezius muscle at 7 T.

Figure 4 shows the difference in temperature distribution on an axial plane passing through the eyes between the CW and GE sequences immediately before and immediately after a single pulse in the GE sequence after 10 min of heating. In each case, the maximum differences are less than 0.001°C.

Time courses for the semianalytical calculations at each individual value of TR followed asymptotic patterns overall with minor variations during each TR, not unlike those shown in Fig. 3. Figure 5 shows the maximum change in temperature during any single repetition for a 2-h long gradient-echo sequence with a pulse duration of 1 ms and a TR varying from 1 (CW) to 5,000 ms in muscle tissue with time-average SAR of 10 W/kg and no thermal conduction.

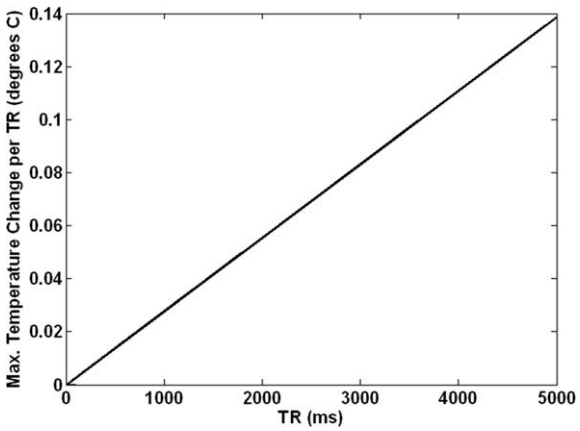

Figure 5 Maximum change in temperature during any single repetition for a 2-h gradient-echo sequence with a pulse duration of 1 ms and a value of TR varying from 1 (CW) to 5,000 ms in muscle tissue with time-average SAR of 10 W/kg as calculated with conservative semianalytical methods allowing for no thermal conduction.

Even in this conservative case (high local SAR with no thermal conduction in tissue with moderate levels of perfusion) for the most extreme case (TR = 5,000 ms with SAR of 50,000 W/kg applied for 1/5,000 of the time) the maximum temperature change during any repetition of less than 0.14°C.

Both Figs. 3 and 4 indicate that the temperatures are slightly higher in the CW sequence immediately before the RF pulse in the GE sequence and slightly higher in the GE sequence immediately after the RF pulse in that sequence. Figure 5 indicates temperature changes during a single repetition for extreme cases with no thermal conduction allowed. Because the maximum differences in temperature between pulse sequences with equivalent time-average SAR and reasonable values of TR shown here are miniscule for typical sequences, it should not typically be necessary to explicitly consider RF pulse sequences in calculation of temperature from RF heating in MRI. This ensures more general applicability of temperature calculation results and allows for larger time steps and faster calculations when using a time-domain approach like those most commonly used (*2–6*, *15*).

ACKNOWLEDGMENT

This work was supported by a funding through NIH grant R01 EB000454 and R01 EB006563.

REFERENCES

1. International Electrotechnical Commission. 2002. 601-2-33: International standard, medical equipment, Part 2: particular requirements for the safety of magnetic resonance equipment for medical diagnosis, 2nd revision. Geneva: International Electrotechnical Commission.
2. Hand JW, Lau RW, Lagendijk JJW, Ling J, Burl M, Young IR. 1999. Electromagnetic and thermal modeling of SAR and temperature fields in tissue due to an RF decoupling coil. J Magn Reson Imaging 42:183–192.
3. Collins CM, Liu W, Wang J, Gruetter R, Vaughan JT, Ugurbil K, et al. 2004. Temperature and SAR calculations for a human head within volume and surface coils at 64 and 300 MHz. J Magn Reson Imaging 19:650–656.
4. Nguyen UD, Brown JS, Chang IA, Krycia J, Mirotznik MS. 2004. Numerical evaluation of heating of human head due to magnetic resonance image. IEEE T Bio-Med Eng 51:1301–1309.
5. Nadobny J, Szimtenings M, Diehl D, Stetter E, Brinker G, Wust P. 2007. Evaluation of MR-induced hot spots for different temporal SAR modes using a time-dependent finite difference method with explicit temperature gradient treatment. IEEE Trans Bio-Med Eng 54:1837–1850.
6. Wang Z, Lin JC, Mao W, Liu W, Smith MB, Collins CM. 2007. SAR and temperature: simulations and comparison to regulatory limits for MRI. J Magn Reson Imaging 26:437–441.
7. Wang Z. 2005. MRI RF coil model design and numerical evaluation using the finite difference time domain method. PhD Dissertation, University of Illinois.
8. Taflove A, Hagness SC. 2005. Computational electrodynamics: the finite-difference time-domain method, 3rd ed. Boston: Artech House Press.
9. Vaughan JT, Hetherington HP, Harrison JG, Otu JO, Pan JW, Pohost GM. 1994. High frequency volume coils for clinical NMR imaging and spectroscopy. Magn Reson Med 32:206–218.
10. Gabriel C. 1996. AL/OE-TR-1996-0037: Compilation of the dielectric properties of body tissues at RF and microwave frequencies. Texas: Brooks Air Force Base: Air Force Materiel Command.
11. Pennes HH. 1948. Analysis of tissue and arterial blood temperatures in the resting human forearm. J Appl Physiol 1:93–122.
12. Wang J, Fujiwara O. FDTD computation of temperature rise in the human head for portable telephones. IEEE T Microwave Theory 1999; 48:528–1534.
13. Wainwright P. 2000. Thermal effects of radiation from cellular telephones. Phys Med Biol 45:2363–2372.
14. Duck FA. 1990. Physical properties of tissue: a comprehensive reference book. London: Academic Press.
15. Wang Z, Collins CM. 2008. On consideration of physiological response in numerical models of temperature during MRI of the human head. J Magn Reson Imaging 28:1303–1308.